Jurnal Teknologi

SIMULTANEOUS ELECTROCHEMICAL DETECTION OF ASCORBIC ACID, DOPAMINE, AND URIC ACID AT MAGNETIC NANOPARTICLES/REDUCED GRAPHENE OXIDE MODIFIED ELECTRODE

Azleen Rashidah Mohd Rosli[a], Farhanini Yusoff[a]*, Saw Hong Loh[a], Hanis Mohd Yusoff[a], Muhammad Mahadi Abdul Jamil[b], Shazrul Hasry Shamsudin[c]
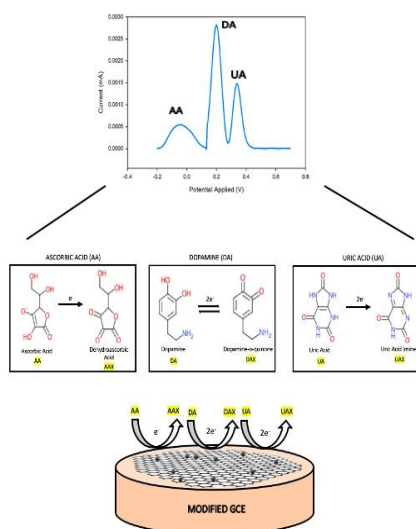
[a]Faculty of Science and Marine Environment, Universiti Malaysia Terengganu, 21030 Kuala Terengganu, Malaysia
[b]Faculty of Electrical and Electronic Engineering, University Tun Hussein Onn Malaysia, Batu Pahat, 86400 Johor, Malaysia
[c]SGS Malaysia Sdn. Bhd., Lot 3 & Lot, 4, Persiaran Jubli Perak, Seksyen 22, 40300 Shah Alam, Selangor, Malaysia

Graphical abstract

Abstract

A magnetic nanoparticles/reduced graphene oxide modified glassy carbon electrode (MNP/rGO/GCE) was fabricated via one-step facile synthesis route for the simultaneous determination of ascorbic acid (AA), dopamine (DA), along with uric acid (UA). A series of diseases and disorders has been associated with irregular levels of these respective analytes, thus early detection is highly crucial. Physical and electrochemical characterization of the modified electrode was conducted by using Scanning Electron Microscopy (SEM), Fourier Transform Infrared (FTIR) analysis, X-Ray Diffraction (XRD) analysis and Brauneur-Emmet-Teller (BET), Cyclic Voltammetry (CV) and Electron Impedance Spectroscopy (EIS). The results obtained confirmed the formation of MNP/rGO composite. Differential pulse voltammetry (DPV) of MNP/rGO/GCE displays three well-defined peaks which associated to AA, DA and UA, respectively. The response towards DA is linear in the concentration range of 15 nM to 100 µM with a detection limit of 0.19 nM while a response to AA and UA is also linear in the concentration range of 10 µM to 100 µM with a limit of detection 0.22 µM and 45 nM respectively. The proposed modified electrode offers a good response towards simultaneous detection of three different electroactive species with excellent electron transfer rate, great capacitance and ideal diffusive control behavior.

Keywords: Ascorbic acid, dopamine, grapheme, magnetic, uric acid

Abstrak

Sebuah elektrod karbon berkaca telah dimodifikasikan dengan magnetik nanopartikel/grafin oksida terturun (MNP/rGO) melalui kaedah sintesis mudah satu langkah untuk penentuan serentak asid askorbik (AA), dopamine (DA) dan asid urik (UA). Tahap kepekatan yang tidak normal bagi setiap analit yang berkaitan boleh menyebabkan serangkaian penyakit dan gangguan. Oleh itu, pengesanan awal analit tersebut adalah sangat penting. Pencirian fizikal dan elektrokimia telah dijalankan untuk elektrod terubahsuai tersebut menggunakan analisis Miksroskop Imbasan Elektron (SEM), Transformasi Fourier InfraMerah (FTIR), Pembalauan X-Ray (XRD), analisis Brunauer-Emmett-Teller (BET), teknik Voltametri Berkitar (CV) dan Spektroskopi Elektrokimia Impedans (EIS). Hasil yang didapati Berjaya membuktikan formasi komposit MNP/rGO. Analisa Voltametri Pembezaan Denyutan (DPV) hasil dari elektrod terubahsuai MNP/rGO telah menunjukkan tiga puncak yang didefinisikan dengan baik yang dipunyai oleh AA, DA dan UA. Tindakbalas terhadap DA yang didapati adalah linear di dalam julat kepekatan antara 15 nM hingga 100 µM dengan had pengesanan 0.19 nM, manakala respon tindakbalas terhadap AA dan UA juga adalah linear di dalam julat kepekatan 10 µM hingga 100 µM. Had pengesanan bagi kedua-dua analit adalah 0.22 µM dan 45 nM. Elektrod terubahsuai yang dicadangkan menawarkan tindak balas yang baik terhadap penentuan serentak tiga spesies elektroaktif yang berbeza dengan mempamerkan pemindahan elekton yang baik, kapasitif yang baik dan juga kelakuan kawal resap yang ideal.

Kata kunci: Asid askorbik, asid urik, dopamin, grafin, dan magnetic

1.0 INTRODUCTION

Ascorbic Acid (AA), Dopamine (DA), and Uric Acid (UA) are vital species in human metabolism physiological activities which usually coexist in the same biological matrices. They are frequently detected in urine, plasma in blood sample, and also extracellular fluid in the body [1]. These respective analytes at abnormally elevated levels can result in a range of diseases and disorders and because these three analytes have similar oxidation potentials, interference from each analyte was presumed. As a result, their sensitive detection is essential not only for biomedical and neurochemical research, but also for diagnostic and pathological studies.

DA is a catecholamine neurotransmitter, a type of chemical being released by nerve cells to send information such as a reward-like pleasure to other neurons and is extensively distributed within the central nervous system of mammalian [2]. The abnormal level of DA will lead to various mental health diseases such as schizophrenia, depression, ADHD along with Parkinson's disease and HIV infection [3,4]. UA is one of the waste products of the purine metabolism in human body, which plays a significant role in brain development by protecting the neuron cells and also functions to control the blood pressure. The significant disease caused by UA is gout, and the irregular level of UA also can cause hyperuricemia, diabetes, high blood pressure as well as high cholesterol [5]. AA or also well known as vitamin C in body has numerous functions in human and animal body. These include wound healing, enhancement of the immune system, formation of collagen, and absorption of ion [6]. AA is vital for the growth, development and repairing of the body's tissue.

In recent past, a few analytical techniques have been developed for the simultaneous determination of AA, DA, and UA which includes chromatography [7], fluorimetry [8], chemiluminescence [9], and capillary electrophoresis mass spectrometry method [10]. Although these approaches offer excellent sensitivity in AA, DA, and UA sensing, they often have limitations, including a complex system, a lengthy analysis time, high analyte consumption, hence the need for improvement over time. As a response, the electrochemical sensing method is an effective option for simultaneously detecting these three analytes since it has a lot of benefits, such as simplicity, quick analysis time, low cost, high selectivity, and real-time detection without reducing its sensitivity.

Graphene is sp^2-hybridized carbon atoms that are tightly packed to form a two-dimensional honeycomb crystal lattice structure. In the application of electrochemical sensor, it is crucial to have an excellent electron transfer property for promoting the ability of some enzymes and exceptional catalytic behavior towards small biomolecules. Graphene with outstanding electron mobility, which the value of 200,000 $cm^2V^{-1}s^{-1}$ at electron density $\sim 2 \times 10^{11}$ cm^{-2} fulfill the important requirement of the electrochemical sensor [11]. Graphene also possesses a high surface area and less weighty graphene chemical sensor is wearable, operates at normal atmospheric pressure and room temperature makes it cost-effective and low environmental impacts material [12].

Magnetite nanoparticles (MNP) or iron oxide, Fe_3O_4, have recently attracted much attention due to their superparamagnetic property, high surface area and, biocompatibility. MNP also possess low toxicity and is an easily found element which resulted in the low-cost production [13]. However, MNP has a few drawbacks such as high energy surface, thus will lead to agglomeration of the element in cluster form. This material is also proved not suitable as a stand-alone material due to its poor conductivity property [14]. Therefore, incorporating magnetite with graphene which possesses high electrical conductivity can enhance the conductivities of hybrid materials and also reduce the agglomeration of materials. It is well established that graphene sheets tend to generate irreversible agglomerates thus making further reaction process difficult. Previous studies have indicated that anchoring nanoparticles to the graphene sheets could inhibit the aggregation of graphene sheets and result in mechanically jammed and exfoliated graphene with high surface area. Meanwhile, magnetite based-electrochemical sensors have shown to be excellent choice for highly sensitive sensing with a linear range of several orders of magnitude. The magnetite nanocomposites with the advantages of the magnetism and the conductivity could be easily adhered to the electrode surface to achieve the direct redox reactions and electrocatalytic behaviors of analytes adsorbed on the modified surface. Thus, it will improve the effective surface area and accelerate the rate of electron transfer across the electrode surface fabricated and will eventually promote the sensitivity and stability of the analytical response.

In this study, a simple yet green and cost-effective approach was used to prepare the magnetite/reduced graphene oxide (MNP/rGO) nanoparticles via in-situ one step synthesis route under room temperature condition. The MNP/rGO modified electrode was then fabricated for further analysis of the simultaneous detection of AA, DA and UA.

2.0 METHODOLOGY

2.1 Synthesis of MNP/rGO Nanoparticles

Graphene Oxide (GO) was firstly prepared via Hummer's method synthesis route with slight modification [15]. The MNP/rGO was then synthesized using co-precipitation technique with a mixture of ferrous chloride and ferric chloride of 1:2 molar ratio. The GO synthesized previously was dispersed with distilled water and undergo sonification process for an hour. Then the iron salt solution was added dropwise onto the GO mixture and ammonium hydroxide which acts as base to control the pH of the solution to pH 10 was added under controlled temperature. Then, a hydrazine hydrate, also known as reductant was slowly dropped onto the mixture to reduce the GO to rGO with constant stirring and elevation of temperature until 85-90°C. The resultant black-coloured precipitate was repeatedly washed with ethanol and deionized water to remove excess ion and for overnight.

2.2 Physical Measurement

The microscopic analysis to study the morphology and the element percentage of the composite were done using the SEM-EDS analysis (JEOL JSM 630 LA). Meanwhile, the analysis of BET was completed using Micrometrics ASAP 2020 with the condition of heating rate 10°C over a range of temperature 30°C to 800°C under the argon atmosphere to study the surface area of the nanoparticles with the pore volume properties. The spectroscopic analysis using FTIR Spectrophotometer (Perkin Elmer 100) and XRD Diffractometer (Rigaku Miniflex II) were used for structural functionalities and formation of the composite with the condition of the spectral range of 2000 to 450cm^{-1} and scan range for 2θ value from 3^0 to 90^0 using the CuKa as the radiation source respectively.

2.3 Electrochemical Measurement

The bare glassy carbon electrode (GCE) with electrode surface area of 0.08 cm^2 was first polished by the '8' method using slurry alumina powder, followed by rinsing with water. The GCE was then immersed in solution of ethanol and distilled water and sonicated for about 10 min to remove the adsorbed particles on the electrode. MNP/rGO powder with mass of 10 mg was dissolved with 10 mL deionized water and sonicate for 10 minutes to obtain a homogeneous solution of MNP/rGO suspension was then drop-casted on top of the GCE surface. At least 7 μL of MNP/rGO suspension was cast onto the GCE.

Electrochemical characterization using cyclic voltammetry and differential pulse voltammetry techniques were used to determine the identification of aspects concerning the redox system process and the transport properties of an electroactive species in the solution. Three electrode systems with modified glassy carbon electrode as the working electrode, platinum wire that act as the auxiliary electrode and reference electrode of Ag/AgCl electrode was used for the analysis. Supporting electrolyte of 1.0 mol of potassium chloride (KCl) and 5.0 mmol of potassium ferrocyanide were used with scan rate of 150 mVs-1 and 6 numbers of scan. The potential range is from -0.2 V to 0.8 V. Electrochemical impedance spectroscopy (EIS) measurements were performed using Autolab instrument equipped with FRA32M and controlled fitness by NOVA 1.10 software under direct potential 0.20 V.

3.0 RESULTS AND DISCUSSION

3.1 Physical Characterization of MNP/rGO Nanoparticles

During the preparation procedure of the MNP/rGO nanoparticles, the formation of Fe_3O_4 nanoparticles was initiated by the strong base when NH_4OH was added to the iron salt mixture and GO that acted as a strong oxidant in the synthesis process aided the deposition of magnetite onto the rGO sheets [16]. This can be proven by the SEM image in Figure 1 with the elemental presence of the prepared MNP/rGO.
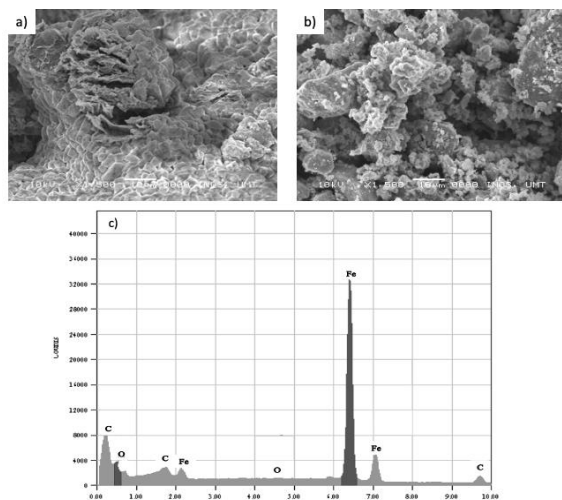

Figure 1 (a) SEM micrograph of MNP/rGO nanoparticles with magnification of x1500 and the operational voltage of 10kV, (b) SEM micrograph of MNP with magnification x1500 with same operational voltage, (c) EDX elemental graph of MNP/rGO

It can be seen that the Fe_3O_4 nanoparticles are well dispersed on the rGO sheets and display uniform deposition patterns along the wrinkle-like rGO surface [Figure 1(a)]. Consistent particle sizes of MNP suggest that the magnetite nanoparticles experienced minimal agglomeration when the particle was incorporated with a larger surface area of rGO [17]. Figure 1(b) display the sphere-shaped structure of MNP where the particles are clustered together with absence of rGO sheets. The EDX elemental graph in Figure 1(c) signifies the presence of element Fe, O and C in the MNP/rGO composite with a percentage of 56%, 18% and 26%, respectively. The result confirmed the existence of high percentage iron element among others and elimination of undesired elements during the synthesis process.

The FTIR spectrum of the synthesized MNP/rGO with comparison with GO particles are shown in Figure 2(a) with a broad peak at the region $3375cm^{-1}$ to $3246cm^{-1}$ which attributed to the stretching vibration of OH group caused by the usage of abundance of water molecules along the synthesis process [18]. The vibration peak of MNP/rGO at $2351cm^{-1}$, $1639cm^{-1}$

and $1460cm^{-1}$ describe the C=C stretch, conjugation of C=O with two aromatic rings that complement the nature of rGO and C-H symmetric stretch respectively. In contrast, the peak at region $536cm^{-1}$ proves the presence of Fe stretch. In comparison, the GO spectrum shows absorption peak of C=O carbonyl stretch, C=O aromatic stretch, C-OH stretch and C-O alkocy stretch at wavelength of $1739cm^{-1}$, $1620cm^{-1}$, $1209cm^{-1}$ and $1041cm^{-1}$ respectively.

XRD analysis (Figure 2b) was practiced to validate the crystalline features with phase structure of the nanoparticles. The analysis was also applied to support the evidence of complete reaction and synthesis process of MNP/rGO nanoparticles. The peak located at 23^0 refers to crystal structure of C (002) from rGO while XRD peaks that appear at 2θ value of 33^0, 36^0, 40^0, 49^0 54^0, 63^0, and 72^0 specify the characteristic of face-centered-cubic (fcc) crystallographic structure of Fe_3O_4 correspond to (311), (222), (400), (422), (511), (620) and (533) respectively [19].
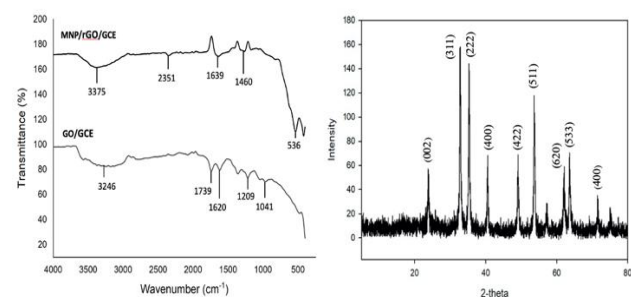

Figure 2 (a) FTIR spectrum of MNP/rGO and GO and (b) XRD Diffractogram of MNP/rGO

BET technique includes external area and pore area evaluations to determine the total specific surface area in m^2/g yielding important information in studying the effects of surface porosity and particle size. BET is used to prove the hypothesis from SEM micrograph, which shows the Fe3O4 nanoparticles being attached to the rGO surface by the increase surface area of the composite [20].

The nitrogen isotherm adsorption plot of rGO, MNP, and MNP/rGO in Figure 3 displays a Type IV isotherm and specify as hysteresis loop by the IUPAC reference where the mesopore composite undergo capillary condensation [21]. The specific pore structure of nanoparticles can be demonstrated by the shape of the hysteresis loop which the three materials exhibit a H3 loop of slit-shaped pores caused by the aggregation of plate-like particles. The pore size, pore volume and surface area of rGO, MNP, and MNP/rGO from Table 1 indicate that the MNP/rGO possesses a low surface area compared to rGO and MNP while the pore volume features is slightly higher than rGO but lower than MNP. This revealed that the low surface area of MNP has been successfully decorated with high surface area rGO that was discussed earlier from the SEM micrograph.
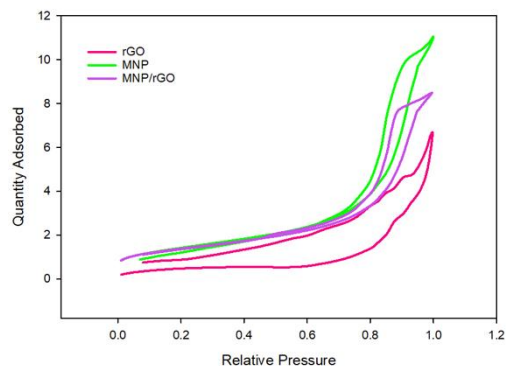
Figure 3 Nitrogen isotherm plot for rGO, MNP, and MNP/rGO

Table 1 Information obtained for BET analysis

Materials	Pore size (nm)	Pore volume (cm³/g)	BET surface area (m²/g)	Langmuir surface area (m²/g)
MNP/rGO	10.77	0.29	109.34	153.60
MNP	13.43	0.38	114.15	160.09
rGO	23.27	0.23	39.63	61.12

3.2 Electrochemical Characterization of MNP/rGO Nanoparticles

The electrochemical behaviour of the modified and unmodified electrode was studied using cyclic voltammetry technique to verify the electron transfer properties of MNP/rGO/GCE in various analyte solutions. Figure 4 signifies the redox peak current of the modified MNP/rGO/GCE has define oxidation peak compared to bare GCE. This means that there is a distinct electron transfer between the redox probe and the electrode surface due to the presence of composite on the GCE. The high electron transfer can also be associated with the composite's high electrical conductivity on the electrode surface.
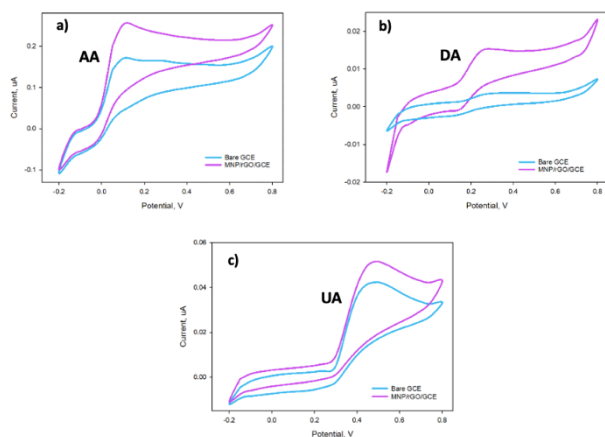

Figure 4 Cyclic voltammogram of comparison different electrode of bare GCE and MNP/rGO/GCE in (a) 100µM of AA standard solution, (b) 100µM of DA standard solution and (c) 100µM of UA standard solution with supporting electrolyte of 0.1M PBS solution (pH7)

The EIS analysis was done to study the electrochemical properties of the electrode which include the electron or charge transfer features between the surface of the electrode and electroactive species in the electrolyte. Nyquist plot of bare GCE, rGO/GCE, MNP/GCE, and MNP/rGO/GCE are displayed in Figure 5(a) obtained at frequency of 1-10000Hz in electrochemical probe of $[Fe(CN)_6]^{-3/-4}$. At high frequency of the Nyquist plot, an obvious semicircle representing the electron transfer resistance (R_{ct}) between the electrochemical active species and electrode surface. Meanwhile, at low frequency section of the graph, a vertical linear part indicates the diffusion behaviour of the modified and unmodified electrode [22]. The result demonstrates that bare GCE has an apparent semicircle suggesting a high impedance while the modified GCE of rGO, MNP and MNP/rGO shows no semicircle observed, indicating a low resistive property owned by the modified GCE. These low resistance properties are believed to help promote the electron transfer rate [23]. Meanwhile, at a low frequency region, a vertical straight line can be monitored for all modified electrode which demonstrates a diffusion behaviour. MNP/rGO/GCE has the highest slope of straight line near the 90° which signifies the response towards the Warburg impedance. The modified Randles equivalent circuit fitted from the Nyquist plot is presented in Figure 5(b) and the circuit-derived parameters are listed in Table 2. The solution resistance (R_s) of MNP/rGO/GCE appear to be the lowest among the modified and unmodified GCE with value of 32.6Ωm² compared to rGO/GCE (43.6Ωm²), MNP/GCE (56.2Ωm²) and bare GCE (69.5Ωm²). The R_s appears to have different value even though same electrolyte being used is due to the use of different modified electrode that exhibits different reactivity of analyte species to the electrode surface. The surface charge and double layer formation between different modified electrode also may influence the solution resistance value [24]. The low R_{ct} value of modified GCE suggest the resistance from the electron transfer via MNP/rGO/GCE is lowest compared to rGO/GCE, MNP/GCE and unmodified bare GCE with value of 14.7Ωm², 38.2Ωm², 75.3Ωm², and 89.0Ωm² respectively. This is proved by the low resistive properties owned by the modified electrode described earlier in the Nyquist plot discussion of high frequency. The Warburg impedance (Z_W) value are distributed as follows: MNP/rGO/GCE (5.36mΩm²) > rGO/GCE (2.48 mΩm²) > MNP/GCE (0.10 mΩm²) > bare GCE (0.07 mΩm²). The Z_W values acquired are supported by the diffusion straight line from the Nyquist plot's low frequency section and reveals that MNP/rGO/GCE with highest Z_W has low diffusion-limiting process at the electrode interface and possess a high diffusive behaviour with an ideal capacitive behaviour [25]. The apparent standard rate constant (K_{app}) of the MNP/rGO is the highest value with 1.42×10^{-8}cms⁻¹ compared to other modified and unmodified GCE. The K_{app} is calculated using Equation 1:

$$K_{app} = (RT/F^2 R_{ct} C) \qquad \text{(Equation 1)}$$

Where C is the concentration of the electroactive species in the electrolyte. The n value of MNP/rGO/GCE (0.89) which is near the pure capacitor value (n=1) signifies the capacitive behaviour of the modified electrode. The bode modulus plot in Figure 5(c) illustrate at low frequency, a lowest impedance value of MNP/rGO/GCE means a high conductive feature. Based on the information gained, it can be concluded that the modified electrode of MNP/rGO/GCE has an excellent conductive property with superior electron transfer feature and exhibit an ideal capacitor behavior.
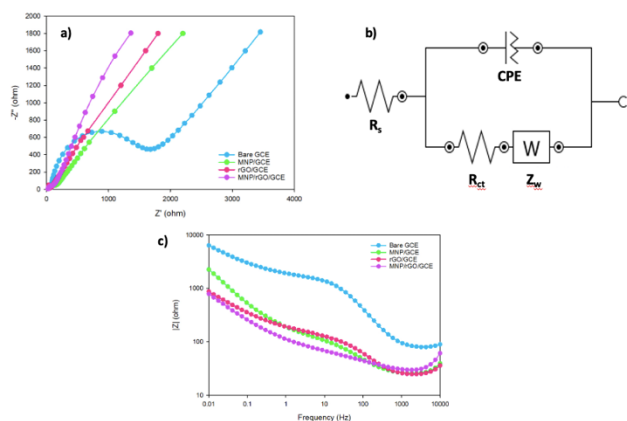

Figure 5. (a) Nyquist plot (b) the modified Randles equivalent circuit, and (c) Bode modulus of the unmodified bare GCE and modified GCE in supporting electrolyte of 1.0M KCl and 5mM $K_4[Fe(CN)_4]$ solution

Table 2 Parameters value of modified Randles equivalent element of the modified electrode

Modified electrode	$R_s/$ Ωm^2	$R_{ct}/$ Ωm^2	$Z_w/$ $m\Omega cm^2$	n	$K_{app}/$ cms^{-1}
Bare GCE	69.5	89.0	0.07	0.52	$5.0e^{-9}$
MNP/GCE	56.2	75.3	0.10	0.76	$4.7e^{-9}$
rGO/GCE	43.6	38.2	2.48	0.79	$7.3e^{-9}$
MNP/rGO/ GCE	32.6	14.7	5.36	0.89	$1.42e^{-8}$

3.3 Simultaneous Detecttion of Ascorbic Acid, Dopamine and Uric Acid

Different modified electrode behavior towards the electrochemical response, when the three different analyte standards of AA, DA and UA were included in the electrolyte of 0.1M PBS solution, can be observed in Figure 6. A three well-separated oxidation peak corresponding to the oxidation reaction of AA, DA, and UA for the MNP/rGO/GCE is more define compared to others suggesting that this modified electrode has high selectivity and able to simultaneously detect three different analytes at the same time in the mixture solution.
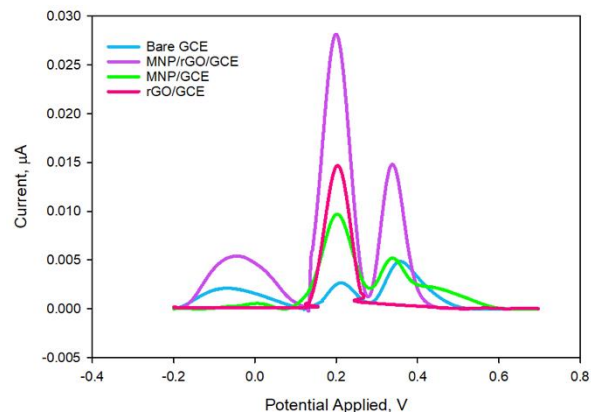

Figure 6 Differential pulse voltammogram of different modified electrode in the standard solution containing 100µM AA, 100µM DA, and 100µM UA electrolyte with supporting solution of 0.1M PBS (pH7)

Figure 7 shows the DPV analysis for the individual determination of AA, DA and UA under parameters of potential range -0.2 V to 0.7 V with scan rate 0.10 V/s in supporting electrolyte of PBS solution with a concentration of 0.1 M and pH 7. This part of study is to identify the resultant oxidation peak potential of AA, DA and UA to confirm the simultaneous detection of reactive molecules without interference from other undesired species and the oxidative peak are between -0.18 V for AA, 0.2 0V for DA and 0.38 V for UA. The linear range used for each analyte varies from 10 µM to 100 µM for AA and UA while the concentration range used for DA is 15 nM to 100 µM. The resultant oxidative peaks observed display that the electrochemical response of each molecule increases linearly with the increase of the analyte's concentration. The R^2 obtained from the linear calibration plot of AA, DA and UA are 0.983, 0.996 and 0.993 respectively.
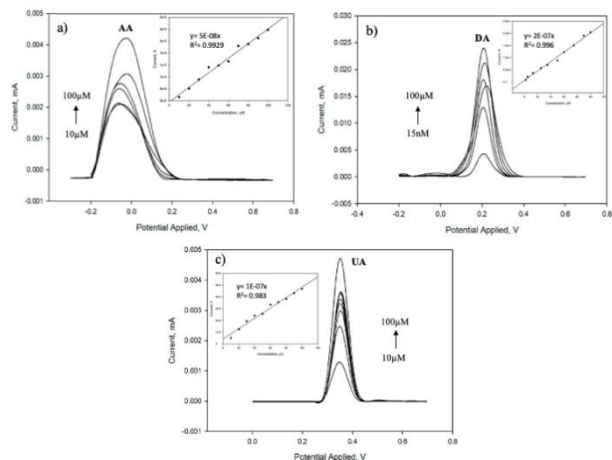

Figure 7 Differential pulse voltammogram of (a) AA standard solution with inset of calibration plot for concentration vs current, (b) DA standard solution with inset of calibration plot for concentration vs current, and (c) UA standard solution with inset of calibration plot for concentration vs current with supporting electrolyte of 0.1M PBS solution (pH7) at potential -0.3 V to 0.7 V

The detection limit (LOD) of an analyte is defined by the lowest concentration of the analyte species that can be detected in the desired sample. The LOD value was calculated using the calibration plot (Figure 7: inset) of the influence of analyte's concentration graph by Equation 2;

$$LOD = (3 \times standard\ error)/slope \quad (Equation\ 2)$$

A comparison with other materials used for simultaneous detection of the selected reactive species with the detection method and the detection limit of each reported study was tabulated in Table 3.

A distinguished analytical performance of the MNP/rGO/GCE also guaranteed a simultaneous detection of coexisting AA, DA, and UA without interference from other species in the matrices [26,27]. Figure 8 illustrates the increasing oxidation DPV response with increasing concentration of the reactive species. The modification of magnetite with rGO provides different properties from those of each individual component. Specifically, rGO can conjugate with various molecules and act as an excellent performance carrier, while magnetite nanoparticles can be highly dispersed on its surface, and the charge transfer at the interface of these hybrid materials can provide a synergistic effect, in this case with dopamine [28, 29]. This allows the electrode of the composite material to have low detection limits.The modified electrode able to selectively separate the three peak current even with distinct concentration, whether low or high concentration of analyte, and this proves the excellent electrocatalytic activity of MNP/rGO influence a high selectivity and sensitivity of the modified electrode.
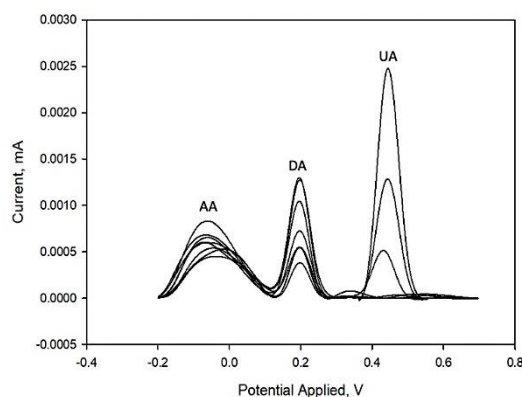

Figure 8 DPV graph for a mixture solution containing varies concentration of the three analytes of AA, DA, and UA at the MNP/rGO/GCE in the supporting electrolyte of 0.1M PBS with neutral pH

Table 3 Comparison study of detection method and electrode materials along with the linear range and detection limit of each analyte

Modified electrode materials	Detection method	Detection limit			Ref
		AA	DA	UA	
AgNPs/rGO	LSV	9.6 µM	5.4 µM	8.2 µM	[6]
Trp-Gr	DPV	10.1 µM	0.29 µM	1.24 µM	[27]
Carboxyl-C_{60}	DPV	-	0.4 nM	5.0 µM	[28]
PMES/rGO	DPV	0.43 µM	0.2 nM	0.56 nM	[1]
GONRs+PEDOT:PSS	DPV	0.41 µM	30.0 nM	11.0 nM	[30]
MNP/rGO	DPV	0.22 µM	0.19 nM	45.0 nM	**This work**

AgNPS (silver nanoparticle); Trp (tryptophan); Gr (graphene); PMES (poly(2-(*N*-morpholine) ethane); GONRs (graphene oxide nanoribbons); PEDOT (poly(3,4-ethylenedioxythiophene)); PSS (polystyrene sulfonate)

4.0 CONCLUSION

In summary, a modified electrode of MNP/rGO/GCE has been successfully synthesized using a simple and environmental-friendly synthesis route of modified co-precipitation technique. The formation of MNP onto the rGO sheets was confirmed via SEM-EDS while the structural functionalities and properties of the materials were studied using FTIR, XRD and BET analysis. Electrochemical analysis of CV and EIS proved that the modified electrode possessed a low diffusion rate with high electron transfer rate. DPV technique was then employed for the simultaneous detection of AA, DA and UA and resulted in the excellent electroanalytical performance exhibited by the MNP/rGO/GCE with a distinguish selectivity within a wide linear range of 10-100µM for both AA and UA along with 15 nM- 100 µM for DA. A low limit of detection obtained for AA, DA and UA are 0.22 µM, 45nM and 0.19 nM respectively.

References

[1] Zhang, H. Z., Zhang, C., Zeng, G. M., Gong, J. L., Ou, X. M., and Huan, S. Y. 2016. Easily Separated Silver Nanoparticle-decorated Magnetic Graphene Oxide: Synthesis And High Antibacterial Activity. *Journal of Colloid and Interface Science.* 471: 94-102.
[2] Olguin, H. J., Guzman, D. C., Garcia, E. H., and Mejia, G. B. 2016. The Role of Dopamine and Its Dysfunction as a Consequence of Oxidative Stress. *Oxidative Medicine and*

Cellular Longevity. 1-13.

[3] Peik-See, T., Pandikumar, A., Nay-Ming, H., Hong-Ngee, L., and Sulaiman, Y. 2014. Simultaneous Electrochemical Detection of Dopamine and Ascorbic Acid Using an Iron Oxide/Reduced Graphene Oxide Modified Glassy Carbon Electrode. *Sensors*. 14(8): 15227-15243.

[4] Nag, A., Mitra, A., and Chandra, S. 2018. Physical Graphene and Its Sensor-based Applications: A Review. *Sensors & Actuatosr: A Physical*. 270: 177-194.

[5] Becker, B. F. 1993. Towards the Physiological Function of Uric Acid. *Free Radical Biological Medicine*. 14(6): 615-631.

[6] Kaur, B., Pandiyan, T., Satpati, B., and Srivastava, R. 2013. Simultaneous and Sensitive Determination of Ascorbic Acid, Dopamine, Uric Acid, and Tryptophan with Silver Nanoparticles-decorated Reduced Graphene Oxide Modified Electrode. *Colloids and Surfaces B: Biointerfaces*. 111: 97-106.

[7] Abdolmohammad-Zadeh, H., Zamani, A., and Shamsi, Z. 2019. Preconcentration of Morphine and Codeine Using a Magnetite/Reduced Graphene Oxide/Silver Nano-Composite and Their Determination by High-performance Liquid Chromatography. *Journal of Chromatography A*, 1590: 2-9.

[8] Liu, X., Tian, M., Gao, W., and Zhao, J. 2019. A Simple, Rapid, Fluorometric Assay for Dopamine by in Situ Reaction of Boronic Acids and cis -Diol. *Journal of Analytical Methods in Chemistry*. 2019: 1-7.

[9] Zhang, Y., Yin, H., Jia, C. B., Dong, Y. P., Ding, H. C., and Chu, X. F. 2020. Electrogenerated Chemiluminescence of Ru(bpy)$_3^{2+}$ at MoS$_2$ Nanosheets Modified Electrode and Its Application in the Sensitive Detection of Dopamine. *Spectrochimica Acta - Part A: Molecular and Biomolecular Spectroscopy*. 240.

[10] Yusoff, F., Rosli, A.R., & Ghadimi, H. 2021. Synthesis and Characterization of Gold Nanoparticles/Poly3,4-Ethylene-Dioxythiophene/Reduced Graphene Oxide for Electrochemical Detection of Dopamine. *Journal of Electrochemical Society*. 168(2): 26509-26519.

[11] Yazid, N. A. and Joon, Y. C. 2019. Co-precipitation Synthesis of Magnetic Nanoparticles for Efficient Removal of Heavy Metal from Synthetic Wastewater. *AIP Conference Proceedings*. 2124.

[12] Karimi, S., and Rezania H. 2019. Effect of Magnetic Field on Specific Heat and Magnetic Susceptibility of Biased Bilayer Graphene: A Full Band Approach. *Chemical Physics*. 525(6): 110417.

[13] Liu, M., Zhang, X., Wu, W., Liu, T., Liu, Y., Guo, B., and Zhang, R. 2019. One-step Chemical Exfoliation of Graphite to ~100% Few-layer Graphene with High Quality and Large Size at Ambient Temperature. *Chemical Engineering Journal*. 355: 181-185.

[14] Weng, Y. K., Rosli, A. R. M., and Yusoff, F. 2019. Magnetite Graphene for Electrochemical Determination of Uric Acid. *Malaysian Journal of Analytical Sciences*. 23(3): 407.

[15] Prasanna, L., Reddy, J., and Rao, R. 2019. A Comprehensive Review of Applications of Magnetic Graphene Oxide-based Nanocomposites for Sustainable Water Purification. *Journal of Environmental Management*. 231: 622-634.

[16] Vinodha, G., Shima, P. D., and Cindrella, L. 2018. Mesoporous Magnetite Nanoparticle-decorated Graphene Oxide Nanosheets for Efficient Electrochemical Detection of Hydrazine. *Journal of Materials Science*. 54: 4077-4088.

[17] Filik, H., Avan, A. A., and Aydar, S. 2016. Simultaneous Detection of Ascorbic Acid, Dopamine, Uric Acid and Tryptophan with Azure A-interlinked Multi-walled Carbon Nanotube/Gold Nanoparticles Composite Modified Electrode. *Arabian Journal of Chemistry*. 9(3): 471-480.

[18] Albers, R. F., Bini, R. A., Souza, J. B., Machado, D. T., and Varanda, L. C. 2019. A General One-pot Synthetic Strategy to Reduced Graphene Oxide (rGO) and rGO-nanoparticle Hybrid Materials. *Carbon*. 143: 73-84

[19] Park, C. M., Heo, J., Wang, D., Su, C., and Yoon, Y. 2018. Heterogeneous Activation of Persulfate by Reduced Graphene Oxide–elemental Silver/magnetite Nanohybrids for the Oxidative Degradation of Pharmaceuticals and Endocrine Disrupting Compounds in Water. *Applied Catalysis B: Environmental*. 225: 91-99.

[20] Lagrow, A. P., Besenhard, M. O., Hodzic, A., Sergides, A., Bogart, L. K., Gavriilidis, A., and Thanh N. T. K. 2019. Unravelling the Growth Mechanism of the Co-precipitation of Iron Oxide Nanoparticles with the Aid of Synchrotron X-Ray Diffraction in Solution. *Nanoscale*. 11(14): 6620-6625.

[21] Brunauer, S., Emmett, P. H., and Teller, E. 1938. Adsorption of Gases in Multimolecular Layers. *Journal of American Chemical Society*. 60(2): 309-319.

[22] Rosli, A. R., Loh, S. H., and Yusoff, F. 2019. Synthesis and Characterization of Magnetic Fe$_3$O$_4$/Reduced Graphene Oxide and its Application in Determination of Dopamine. *Asian Journal of Chemistry*. 31(12): 2785-2792.

[23] Yusoff, F., Mohamed, N., Azizan, A., and Ghani, S. A. 2016. The perovskite Ba$_{0.5}$Sr$_{0.5}$Co$_{0.2}$Fe$_{0.8}$O$_3$-MWCNT Modified Glassy Carbon Electrode- Its Characterization and Capacity in Oxygen Reduction Reaction. *International Journal of Electrochemical Sciences*. 11(9): 5766-5780.

[24] Yusoff, F., Khing, N. T., Hao, C. C., Sang, L. P., Muhamad, N. B., and Salleh, N. M. 2018. The Electrochemical Behaviour of Zinc Oxide/Reduced Graphene Oxide Composite Electrode in Dopamine. *Malaysian Journal of Analytical Sciences*. 22(2): 227-237.

[25] Muhamad, N. B., Khairul, W. M., and Yusoff, F. 2019. Synthesis and Characterization of Poly(3,4-ethylenedioxythiophene) Functionalized Graphene with Gold Nanoparticles as a Potential Oxygen Reduction Electrocatalyst. *Journal of Solid State Chemistry*. 275: 30-37.

[26] Suhanto, R. N., Rahmawati, R., Setyorini, D. A., Noviandri, I., Suyatman, and Yuliarto, B. 2018. Modified Working Electrode by Magnetite Nanocomposite for Electrochemical Sensor Application. *IOP Conference Series: Material Science and Engineering*. 367: 12054.

[27] Lian, Q., He, Z., He, Q., Luo, A., Yan, K., Zhang, D., Lu, X., and Zhou, X. 2014. Simultaneous Determination of Ascorbic Acid, Dopamine and Uric Acid Based on Tryptophan Functionalized Graphene. *Analytica Chimica Acta*. 823: 32-39.

[28] Tan, J. S., Zhang, X. L., Yu, B., Yuan, H., Cong, H. L., Hao, T. Z., and Wang, C. Q. 2015. Simultaneous Detection of Ascorbic Acid, Dopamine and Uric Acid Using Carboxyl-C60 Modified Electrodes. *Integrated Ferroelectrics*. 162(1): 62-68.

[29] Muhamad, N. A. B., and Yusoff, F. 2018. The Physical and Electrochemical Characterization of Gold Nanoparticles Supported PEDOT/Graphene Composite as Potential Cathode Material in Fuel Cells. *Malaysian Journal of Analytical Sciences*. 22(6): 921-930.

[30] Su, C. H., Sun, C. L., and Liao, Y. C. 2017. Printed Combinatorial Sensors for Simultaneous Detection of Ascorbic Acid, Uric Acid, Dopamine, and Nitrite. *ACS Omega*. 2(8): 4245-4252.